THE DEVELOPMENT OF CFD METHODS FOR ROTOR APPLICATIONS

F. X. Caradonna and W. J. McCroskey

U.S. Army Aeroflightdynamics Directorate (ARTA)
Ames Research Center
Moffett Field, CA 94035-1099

The optimum design of the advancing helicopter rotor for high-speed forward flight always involves a tradeoff of transonic and stall limitations. However, the preoccupation of the rotor industry was primarily concerned with stall until well into the 1970s. This emphasis on stall resulted from the prevalent use of low-solidity rotors with rather outdated airfoil sections. The use of cambered airfoil sections and higher-solidity rotors substantially reduced stall and revealed the advancing transonic flow to be a more persistent limitation to high-speed rotor performance. Work in this area was spurred not only by operational necessity but also by the development of a new tool for the prediction of these flows--the methods of computational fluid dynamics (CFD). The development of CFD for these rotor problems has been a major Army and NASA achievement--accomplished mainly via the original joint Army/NASA agreement at Ames Research Center. This work is now being extended to other rotor flow problems. These developments are outlined in the following discussion.

Development of Rotor Flow Codes

The first Army research on transonic flow began at NASA Ames Research Center in 1970 and closely followed the rapid developments in CFD work at NASA--most notably the work of Steger and Lomax (ref. 1). The first transonic rotor computations, those of Caradonna and Isom (ref. 2), came from this Army research. These computations involved the casting of the potential equation in blade-fixed rotating coordinates and then invoking the classical small perturbation approximation. Solutions were obtained by using the recently developed mixed differencing approach. These were steady, three-dimensional relaxation solutions of nonlifting hovering rotors with rectangular planforms. These computations revealed the onset and development of shocks with increasing radius. The tip relief of these shocks was also shown to be strongly affected by the aspect ratio (fig. 1). This work was extended by Ballhaus and Caradonna (ref. 3) to the treatment of nonrectangular planforms. This work had significant design implications in that it demonstrated that the proper choice of profile and planform are strongly interdependent on one another (fig. 2). The Army computational program was extended by Caradonna and Isom (ref. 4) to the treatment of unsteady flows in 1975. In this work the unsteady three-dimensional, small-disturbance-potential equation was solved. This work was unusual for unsteady solutions in that it used relaxation methods, that is, each time step was solved iteratively. It was shown by this means that transonic flows

are intrinsically unsteady and even a nonlifting transonic rotor flow displays considerable unsteadiness due to the varying incident Mach number that an advancing rotor encounters (fig. 3).

These unsteady computations demonstrated the importance of unsteadiness to the transonic rotor problem. However, the solution method was not very efficient. A more promising approach to unsteady transonic computations was soon developed by Ballhaus and Steger (ref. 5). Their approach was to perform a time linearization of the small perturbation equations. This linearization obviated the need for iteration because the nonlinear coefficients were completely determined by the previous time-step. They further streamlined the method by replacing the relaxation solution with an approximate factorization (AF) algorithm which was applied to the low frequency form of the transonic small-perturbation equations. The AF approach was much faster than relaxation because it imposed no limits on the speed of propagation of numerical information. This approach was soon applied to rotor problems by Caradonna and Philippe (ref. 6). This paper was significant on two accounts: (1) It described rotor computations which simulated the full unsteady-rotor environment, that is, with unsteadiness caused by both Mach number and angle of attack variation (fig. 4). (2) Actually, the most important facet of this paper is that it contained the first experimental confirmation of the unsteady transonic computations (fig. 5). By 1980, this work had been extended to three dimensions (refs. 7, 8) and the development of small perturbation algorithms had essentially reached its present state. Further computational algorithm developments required more exact flow models.

The obvious next step was the development of a full-potential rotor code. This was first accomplished by Arieli and Tauber (ref. 9), who cast the nonconservative, steady full-potential equation in rotating coordinates and modified the fixed wing code, FL022, to obtain solutions. The resulting code, called ROT22, is probably the most-used finite-difference code in the rotor industry. Its limitation to quasi-steady solutions has not diminished its usefulness to various comparative design studies. However, unsteady full-potential codes have since been developed. One of these codes, developed by Chang, is the outgrowth of a quasi-steady code, TFAR1 (ref. 10), which solves the same nonconservative equation as in the ROT22 code. However, whereas ROT22 used a relaxation procedure, TFAR1 uses an approximate factorization approach. Not only is the AF scheme more efficient, but it is readily extended to include the unsteady terms. This has been done in the code TFAR2 (ref. 11, 12). All of the above full-potential treatments have been nonconservative, that is, mass conservation cannot be guaranteed at shocks. This problem was solved in 1980 by Steger (ref. 13) with the development of an AF algorithm to solve the unsteady, conservative full-potential equations. This algorithm was subsequently developed into the fixed wing code, TUNA, by Bridgeman in 1982 (ref. 14). This code was finally developed into the full-potential rotor code, FPR, by Strawn (ref. 15) in 1986. The code FPR represents the latest and most complete of all the potential rotor codes. Its main limitation (like all potential methods) is an inability to treat shock-induced vorticity or very strong (involving separation) blade/vorticity interactions. For these problems Euler and Navier-Stokes methods are necessary.

Euler rotor codes are still in their infancy. However, a very promising beginning is to be seen in the work of Chang (ref. 16). He has used a centered finite-volume approach to solve the Euler equations in the blade-fixed coordinate frame.

To summarize rotor code development, one must say that it has followed the fixed wing work and has progressed unabated for the past fifteen years. As a result, there are several available codes. The small disturbance code, FDR, which is the simplest and most efficient, models the essential unsteady physics and is accurate for high-Mach-number low-lift solutions. The ROT22 and TFAR1 codes (quasi-steady nonconservative) are the best codes to handle high lift solutions where unsteady effects are not dominant. As TFAR2 is an unsteady code, it has no such limitation; it has produced excellent unsteady results in spite of its nonconservative formulation. The problem of nonconservative formulation has been rectified in the code FPR, which is the most general full-potential code, and is readily available. These potential codes are by far the fastest approach to predict transonic flows. However, for problems entailing very strong shocks or requiring detailed modeling of the near wake, Euler and Navier stokes methods are required and are under advanced development. TFAR3 (ref. 16) is an outstanding example of this line of development. There is now no lack of available codes. What is required now is the development of the techniques to use these codes in the overall rotor-flow-prediction process.

Prediction and Verification of Operational Rotor Flows

The early nonlifting rotor computations could be easily handled by simple grids designed to resolve flow features in the immediate vicinity of the blade surface (fig. 6). At present, all available codes still use such blade-localized grids. Nevertheless, any lifting rotor flow is dominated by a wake system which cannot be contained in such a grid. Figure 7 illustrates the problem for a simple hover flow--the first flow for which this problem was rigorously treated. As indicated in figure 7, several vortices from the wake system may pass through the finite difference grid, but the wake system outside of the grid is significant and must be accounted for. This problem was treated by finding (and including in the boundary conditions) the blade-surface normal velocity induced by this outer wake and then solving the local rotor flow in a manner which includes near-blade vortices. These near vortices have been included in several ways. In reference 17, these vortices were treated by imposing branch cuts, the edges of which were at the required vortex locations. A more general approach (ref. 15) is to reformulate the problem so as to find a blade-induced perturbation about a known vortex-induced velocity distribution. These approaches have been validated by comparison with the hover data of reference 18, which is presently the only supercritical rotor surface-pressure data for which simultaneous wake data are also available. The imposition of this measured wake in these codes has resulted in the excellent comparisons shown in figure 8. Subsequent to these comparisons, excellent comparisons (ref. 16) with these hover data have been obtained solely by the use of an inflow boundary condition. This approach is especially useful in a forward flight computation where the use of a near-field vortex model becomes quite tedious due to the time- and

space-varying vortex geometry relative to the blade. This approach was initially employed in the first true self-trimming, finite-difference rotor computation of Tung, Caradonna and Johnson (ref. 19). This computation was performed by combining the small disturbance code (ref. 8), FDR, with CAMRAD (ref. 20) a complete rotor comprehensive code which employs a detailed vortex wake representation. These codes were coupled by using CAMRAD to determine the blade motion and inflow (in the form of an effective angle of attack) resulting from all of the wake except for the vortex sheet contained in the FDR grid (fig. 9). The loads thus obtained by FDR then determined the vortex filament strengths. This coupling was also marked by an iterative scheme which obviated the need to compute the blade dynamics at every finite-difference time step. The resulting scheme is very efficient and will probably form the basis of future high-speed rotor computations. The above coupling procedure has since been applied using several of the NASA and Army codes including FPR and TFAR2. Figure 10 shows a comparison (ref. 21) of several codes with model operational loads survey (OLS) pressure data. Comparisons of CAMRAD/FPR computations with pressure data from an ONERA three bladed rotor are shown in figure 11. These and many other computations have demonstrated the effectiveness of this approach. Similar comparisons with full-scale flight test data are due for release within the year. It is clear that this analysis method should be highly effective for high-speed-rotor design.

It should be understood that these advancing computations use an approximate vortex model (that is, the use of a surface inflow induced by the wake vorticity). This approximation seems to work well for high advance-ratio conditions in which the wake of previous blades is well removed from the rotor. However, a sizable number of relatively high advance-ratio cases are known where the rotor wake is close and strong enough to induce considerable vibratory airloading. This problem has spurred a number of recent efforts to perform more exact computational treatments of blade vortex interactions (BVI).

Blade Vortex Interaction

The strong interaction between a segment of a rotor blade and concentrated tip vortices in the wake is an important source of noise and vibration at low and moderate flight speeds. The limiting case of a vortex intersecting a rotor blade with its axis parallel to the leading edge of the blade, while fundamentally unsteady, is relatively simple for theoretical and numerical analysis, and it has been the subject of several recent investigations. These studies, which were reviewed recently in more detail by Srinivasan and McCroskey (ref. 22), have established the basic features of blade-vortex interactions, and they provide a choice among alternative methods that range from transonic small-disturbance to Navier-Stokes formulations for calculating such interactions.

Within this hierachy of equations and solution algorithms, three basic methods of introducing a concentrated vortex into a computational domain have been employed. The most straightforward approach is (1) to specify initially the complete velocity and pressure field produced by the vortex when it is some distance upstream of the

blade, and then (2) to rely on the properties of the numerical method to maintain the correct vortex structure, and (3) to compute the subsequent interaction as the solution advances in time. Unfortunately, most numerical methods include artificial, numerical dissipation to improve their stability and convergence properties. As a result, the steep gradients within the vortex are diffused more rapidly by the numerics than by physical viscosity, unless excessively fine computational grids are used, and the computed blade-vortex interaction is seriously weakened and in error. Only within the past few months has a numerical scheme emerged that overcomes this difficulty, that of Rai (ref. 23), which is described later.

Consequently, two alternate methods were developed in previous years, in which the vortex is modeled to some extent. (1) The first of these was the branch-cut method (ref. 17), which can be used for potential flows. In addition to the usual branch cut that extends downstream of the trailing edge of the airfoil, a second branch cut is introduced between the vortex and an outer boundary of the flow field, and a jump in velocity potential equal to the strength of the vortex is prescribed across this second branch cut. The flow remains irrotational outside the airfoil and vortex branch cuts, and the governing equation and boundary conditions remain unchanged. However, if the vortex moves through the flow field, the logic of the numerical code must allow its branch cut to move accordingly. The numerical calculations seem to be sensitive to this motion, especially for strong interactions.

(2) The second approach is the prescribed-disturbance method, sometimes called the dual or split-potential method, although it is not restricted to potential flow. In this approach, the velocity field is split into a prescribed part, which represents the "free stream" plus an isolated vortex moving through the flow field, and the remainder that is to be determined and which results from the interaction of the vortex and the airfoil or blade. The resulting finite-difference equations are slightly more complicated, and the entire vortex field must be computed at every grid point and at every time step, thereby increasing the CPU time slightly. However, the method is stable and accurate, and an arbitrary vortex-core structure can be prescribed. The principal limitation of both modeling methods is that they ignore any changes in the structure of the vortex caused by the encounter with the blade. Rai's method (ref. 23) has no such restriction, and, as will be shown later, he has been able to compute a head-on collision between a vortex and an airfoil.

Representative two-dimensional results from References 22 and 25 are shown in figures 12 and 13 for a symmetrical airfoil section at transonic speeds. Figure 12 shows the distortions in the chordwise pressure distributions on the airfoil as the vortex passes underneath, computed by a thin-layer Navier-Stokes code with a solution-adaptive grid, which greatly improves the resolution by placing the most grid points in the regions of highest gradients. The changes in the grid with time are shown in the middle of the figure, and the Mach contours at the bottom help to delineate the flow-field details. These results illustrate that strong gradients in pressure occur with respect to both time and space, because of the vortex encounter. These gradients can be especially significant in the leading-edge region of a thin airfoil.

Figure 13 compares the fluctuating lift on the airfoil computed by transonic small-disturbance (ref. 22) (George, A. R. and Lyrintzis, A., private communication, Moffett Field, CA), full-potential (ref. 25), Euler (Sankar, N. L., Tang, W., and Hsu, T., private communication, Moffett Field, CA) and thin-layer Navier-Stokes codes (ref. 24) at Ames and elsewhere (refs. 22, 25, 26). This is a case with strong nonlinear and unsteady effects, but not severe enough to include boundary-layer separation. The various results are approximately the same for lift, although the instantaneous pressure distributions and shock-wave positions differ more (ref. 22).

The aforementioned head-on encounter, computed by Rai (ref. 23) with a Navier-Stokes code, is shown in figure 14. The vorticity contours indicate the vortex itself and the viscous boundary layer next to the airfoil, and the splitting of the vortex above and below the airfoil is clearly evident. Although there is no shock wave in this subsonic case, this kind of head-on interaction can currently be treated only by this code. The main disadvantage of this code is that it takes about two or three times as much CPU time than the prescribed-disturbance Navier-Stokes code on a comparable grid, and at least 50 times more than the transonic small-disturbance code.

The computational efficiency of the small-disturbance codes means that many more calculations can be performed on a given computational grid, or that much finer grids can be used without excessive CPU costs. This, in turn, has led to their use in exploring the radiating pressure field several chord-lengths away from the airfoil, i.e., BVI noise. Baeder et al. (ref. 26) combined CFD and aeroacoustics concepts in studying this problem, producing the results shown in figure 15. These disturbance-pressure contours exhibit a fidelity unmatched in other investigations. Their results indicate a dramatic sensitivity of the radiated sound to Mach number, but a surprising insensitivity to airfoil shape. Continuing research on this subject is employing other codes and computational grids.

The step from two dimensions to three is enormous, but it must be made for practical rotorcraft problems. The first efforts were by Strawn and Tung (ref. 27), who used a full-potential code to examine special experimental cases run at the Aeroflightdynamics Directorate (ref. 28). Figure 16 shows the rotor-vortex experiment, and figure 17 is a comparison of computed and measured pressure distributions for a difficult, highly-transonic case. Although the agreement is not perfect, the essence of the phenomenon is clearly captured by the numerical results. Extensions to the pressure field off the blade are under way.

Viscous Transonic Airfoil Characteristics

The NASA-Ames code ARC2D (ref. 29) has been used in reference 30 to calculate the transonic viscous flow of helicopter profiles, based on the thin-layer Reynolds-averaged Navier Stokes equations, with an algebraic eddy-viscosity model to approximate boundary-layer turbulence. Figure 18 shows representive results for combinations of Mach numbers and angles of attack that produce significant nonlinear behavior and shock-wave/boundary-layer interaction. The numerical results reproduce

the experimentally observed airfoil behavior across the transonic regime. Also, the details of the computed flow fields provide new insights into transonic airfoil behavior under conditions for which accurate measurements are difficult to obtain and are often tainted by wall-interference effects.

Figure 18 shows the lift behavior at low angles of attack, including the loss of lift that occurs when significant separation is induced by the shock wave in the Mach number range, $0.83 < M < 0.93$ for the NACA 0012 airfoil. The drag rise in the transonic regime is also shown. The abrupt change in pitching-moment behavior, known as "Mach tuck," is illustrated in figure 19. In all cases, the numerical results seem to be as reliable as wind tunnel data. However, the accurate prediction of maximum C_L remains a formidable challenge.

Tip Vortex Formation

The importance of blade-vortex interactions for rotorcraft has led to many ad hoc attempts to alter the structure of the tip vortices. With the recent advent of several three-dimensional Navier-Stokes pilot codes, computational fluid dynamics offers a new tool for this problem. Preliminary results seem very promising.

Srinivasan et al. (ref. 31) recently examined four planforms of nonrotating wings and computed the details of their tip vortex formation. Fair agreement was obtained with the limited available experimental data, e.g., figure 20, although questions remain concerning the grid resolution and the validity of the turbulence model used.

Figure 21 shows the pressure distributions computed on a swept rotor-blade tip in a nonrotating environment. The beneficial effects of leading-edge sweep were demonstrated by comparisons with the same blade with a straight leading edge and the same taper distribution; this blade had a much stronger shock wave and considerable boundary-layer separation. However, it was found that the tip vortex on the swept-tip blade was much more concentrated and had higher peak velocities that the straight leading-edge blade. Therefore, there appears to be much room for planform optimization when both aerodynamic performance and tip-vortex structure are involved.

Aerodynamics of Complete Rotorcraft Configurations

Computational fluid dynamics is incapable today of treating realistic combinations of rotors and bodies. However, algorithms are constantly improving, the rotorcraft industry is beginning to use and gain valuable experience with modern CFD codes, and supercomputer technology is advancing at a dazzling pace. The principal pacing items are algorithm improvements and adaptations to the peculiar features of rotorcraft, turbulence modeling, vortex wake modeling, grid generation; memory size and speed of current supercomputers, user familiarity in the rotorcraft industry, and management acceptance of the potential of CFD, notwithstanding the substantial investment required in manpower, software, and hardware.

In anticipation of future supercomputer capabilities, the Army and NASA have already begun laying the foundation for eventual computational analysis of complete configurations. A first step is creating computational grids on a combination of rotating blades and a nonrotating body, such as a fuselage or tail fin. Figure 22 shows the most promising grid topology that has emerged so far. Here a zonal, or block, grid strategy is employed, in which body-conforming grids are embedded within rotating and nonrotating cylindrical blocks. The cylinders provide the simplest and most accurate topology for passing computed information across the boundary between the rotating and nonrotating solid bodies, whereas other block topologies are more appropriate for computing the flow near the surfaces and in the near wakes.

Finally, the rotorcraft industry stands to benefit enormously from NASA's investment in computational aerodynamics and supercomputer technology in the National Aerodynamic Simulation program (NAS). This multimillion-dollar large-scale computer system, indicated schematically in figure 23, will provide a national computational capability for NASA, the Department of Defense, industry, other government agencies, and universities. Several rotorcraft projects have already been accepted for the NAS program. The vigorous pursuit of computational aerodynamics for rotorcraft applications will benefit all segments of our industry.

Concluding Remarks

Over the past fifteen years, the Army and NASA research groups at Ames Research Center have developed a wholly new approach to rotor flow prediction. This work has included the development of a number of rotary wing computational fluid dynamics (CFD) codes, which are now seeing extensive industrial use. With these codes it is now practical to perform many complete rotor computations which include transonic unsteady and three-dimensional effects without recourse to empiricisms and extensive data libraries. These tools permit a new level of high-speed-rotor design capability.

Although the high-speed-flow methods are now becoming operational, there are a number of significant flow problems which remain and can best be treated by CFD. Stall is one of the foremost of these problems. Although this problem has been neglected of late, it remains the primary limiter to rotor lifting capability. New Navier-Stokes codes will ultimately permit an understanding of three dimensional stall effects. Another area which requires much work concerns interactional aerodynamics, including various blade-vortex, main-rotor/tail-rotor and rotor-fuselage interactions. A developing understanding and ability to predict these effects will enable substantial control and design for vibratory loading.

The potential payoff for future rotor CFD developments remains high. As in the past, however, these developments will require the combination of computational, experimental, and operational capabilities which are found in the Army and NASA rotor research organizations.

References

1. Steger, J. L.; and Lomax, H.: Transonic Flow About Two-Dimensional Airfoils by Relaxation Procedures. AIAA J., vol. 10, no. 1, Jan. 1972, pp. 49-54.

2. Caradonna, F. X.; and Isom, M. P.: Subsonic and Transonic Potential Flow Over Helicopter Rotor Blades. AIAA J., vol. 10, Dec. 1972, pp. 1606-1612.

3. Ballhaus, W. F.; and Caradonna, F. X.: The Effect of Planform Shape on the Transonic Flow Past Rotor Tips. Aerodynamics of Rotary Wings, AGARD CP-111, Feb. 1973.

4. Caradonna, F. X.; and Isom, M. P.: Numerical Calculation of Unsteady Transonic Potential Flow Over Helicopter Rotor Blades. AIAA J., vol. 14, no. 4, Apr. 1976.

5. Ballhaus, W. F.; and Steger, J. L.: Implicit Approximate Factorization Schemes for the Low-Frequency Transonic Equation. NASA TM X-73082, Nov. 1975.

6. Caradonna, F. X.; and Philippe, J. J.: The Flow Over a Helicopter Blade Tip in the Transonic Regime. Vertica, vol. 2, 1978, pp. 43-60.

7. Caradonna, F. X.; and Steger, J. L.: Implicit Potential Methods for the Solution of Transonic Rotor Flows. Proceedings of the Army Numerical Analysis and Computers Conference. ARO Rep. 80-3, Aug. 1980.

8. Chattot, J. J.: Calculation of Three-Dimensional Unsteady Transonic Flows Past Helicopter Blades. NASA TP-1721, 1980.

9. Arieli, R.; and Tauber, M. E.: Computation of Subsonic and Transonic Flow About Lifting Rotor Blades. AIAA Paper 79-1667, Aug. 1979.

10. Chang, I-Chung: Transonic Flow Analysis for Rotors - Part I. Three-Dimensional, Quasi-Steady, Full-Potential Calculation. NASA TP-2375, 1984.

11. Chang, I-Chung: Transonic Flow Analysis for Rotors - Part II. Three-Dimensional, Unsteady, Full-Potential Calculation. NASA TP-2375, 1985.

12. Chang, I-Chung; and Tung, C.: Numerical Solution of the Full-Potential Equation for Rotors and Oblique Wings Using a New Wake Model. AIAA Paper 85-0268, Jan. 1985.

13. Steger, J. L.; and Caradonna, F. X.: A Conservative Implicit Finite Difference Algorithm for the Unsteady Transonic Full Potential Equation. AIAA Paper 80-1368, Snowmass, CO, 1980.

14. Bridgeman, J. O.; Steger, J. L.; and Caradonna, F. X.: A Conservative Finite-Difference Algorithm for the Unsteady Transonic Potential Equation in Generalized Coordinates. AIAA Paper 82-1388, Aug. 1982.

15. Strawn, R. C.; and Caradonna, F. X.: Numerical Modeling of Rotor Flows with a Conservative Form of the Full-Potential Equations. AIAA Paper 86-0079, Jan. 1986.

16. Chang, I. C.; and Tung, C.: Euler Solution of the Transonic Flow for a Helicopter Rotor. AIAA Paper 87-0523, AIAA 25th Aerospace Sciences Meeting, Jan. 1987.

17. Caradonna, F. X.; Desopper, A.; and Tung, C.: Finite Difference Modeling of Rotor Flows Including Wake Effects. J. Am. Hel. Soc., vol. 29, no. 2, Apr. 1984.

18. Caradonna, F. X.; and Tung, C.: Experimental and Analytical Studies of a Model Helicopter Rotor in Hover. NASA TM-81232, 1981.

19. Tung, C.; Caradonna, F. X.; and Johnson, W. R.: The Prediction of Transonic Flows on an Advancing Rotor. AHS J., vol. 31, no. 3, July 1986, pp. 4-9.

20. Johnson, W.: A Comprehensive Analytical Mode of Rotorcraft Aerodynamics and Dynamics, Part 1, Analysis Development. NASA TM-81182, 1980.

21. Caradonna, F. X.; and Tung, C.: A Review of Current Finite Difference Rotor Flow Methods. AHS 42nd Annual Forum Proceedings. June 2-4, 1986, Washington, DC.

22. Srinivasan, G. R.; and McCroskey, W. J.: Numerical Simulations of Unsteady Airfoil-Vortex Interactions. Vertica, vol. 10, no. 5, 1986.

23. Rai, M. M.: Navier-Stokes Simulations of Blade-Vortex Interaction Using High-Order Accurate Upwind Schemes. AIAA Paper 87-0543, 1987.

24. Srinivasan, G. R.; McCroskey, W. J.; and Baeder, J. D.: Aerodynamics of Two-Dimensional Blade-Vortex Interaction. AIAA J., vol. 24, no. 10, pp. 1569-1576, Oct. 1986.

25. Jones, H. E.; and Caradonna, F. X.: Full-Potential Modeling of Blade-Vortex Interactions. 12th European Rotorcraft Forum, Paper no. 27, Sept. 1986.

26. Baeder, J. D.; McCroskey, W. J.; and Srinivasan, G. R.: Acoustic Propagation Using Computational Fluid Dynamics. AHS 42nd Annual Forum, Washington, June 1986.

27. Strawn, R. C.; and Tung, C.: The Prediction of Transonic Loading on Advancing Helicopter Rotors. AGARD CP-412, Paper no. 7, 1986.

28. Caradonna, F. X.; Tung, C.; and Laub, G.: An Experimental Study of the Parallel Blade Vortex Interaction. 10th European Rotorcraft Forum, The Hague, Netherlands, Aug. 1984.

29. Pulliam, T. H.; and Steger, J. L.: Recent Improvements in Efficiency, Accuracy, and Convergence for Implicit Approximate Factorization Algorithms. AIAA Paper 85-0360, 1985.

30. McCroskey, W. J.; Baeder, J. D.; and Bridgeman, J. O: Calculation of Helicopter Airfoil Characteristics for High-Tip Speed Applications. J. AHS, vol. 31, no. 2, pp. 3-9, Apr. 1986.

31. Srinivasan, G. R.; McCroskey, W. J.; Baeder, J. D.; and Edwards, T. A.: Numerical Simulation of Tip Vortices of Wings in Subsonic and Transonic Flow. AIAA Paper 86-1095, May 1986.

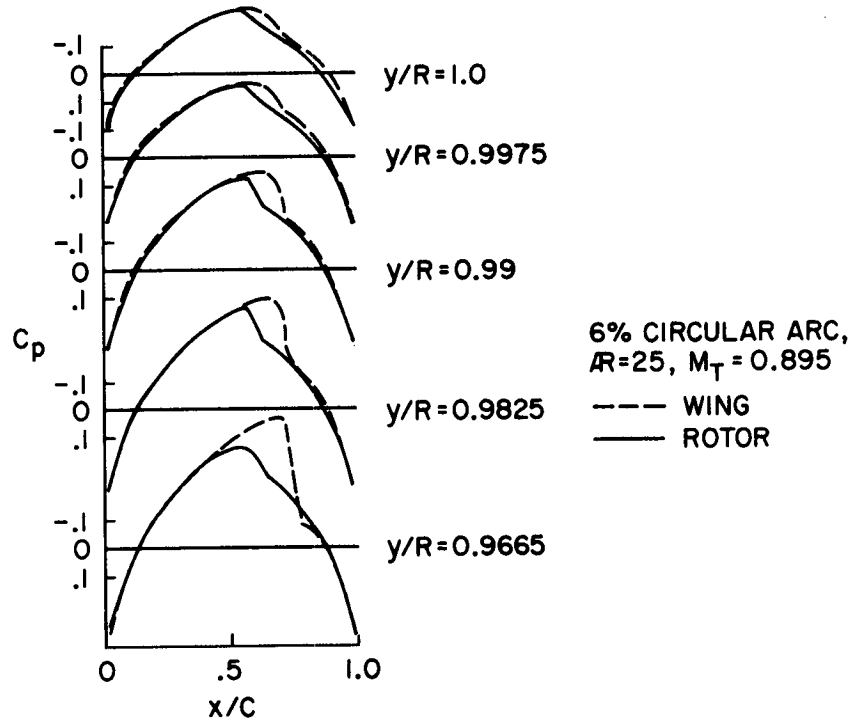

Figure 1(a).- Comparison of wing and rotor transonic flows. Such studies were first made possible by the development of CFD in the early 1970s.

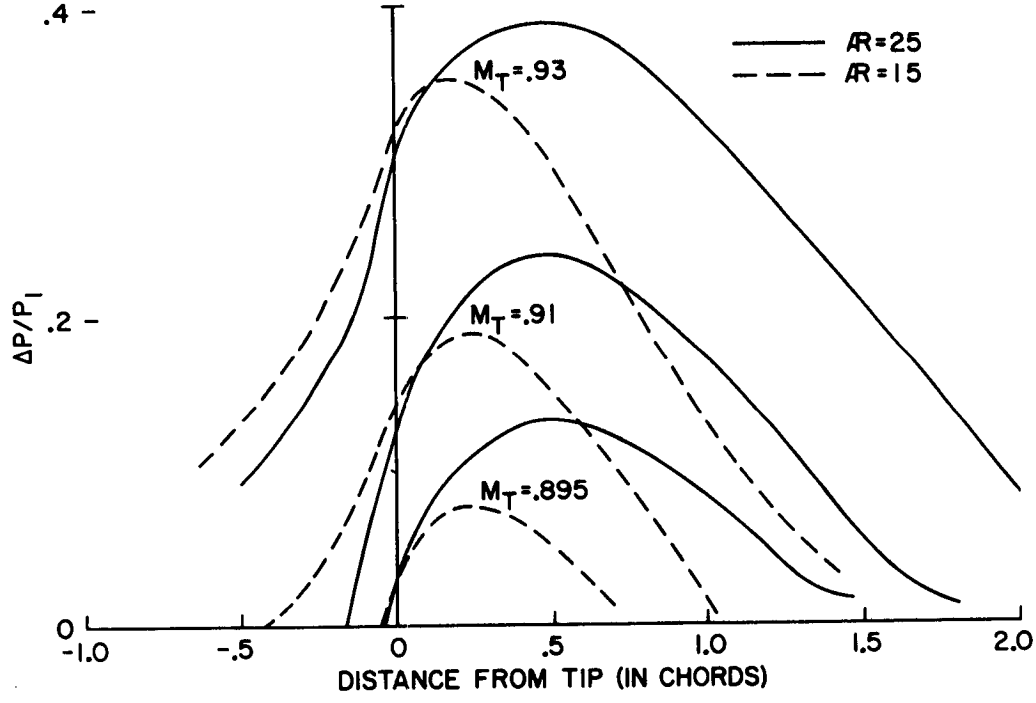

Figure 1(b).- Comparison of shock strength as functions of aspect ratio, rotor radius, and tip Mach number. The lower aspect ratios produce weaker shocks on the blade but stronger shocks off the blade. This early computational result has performance and acoustic implications which are not yet fully realized today.

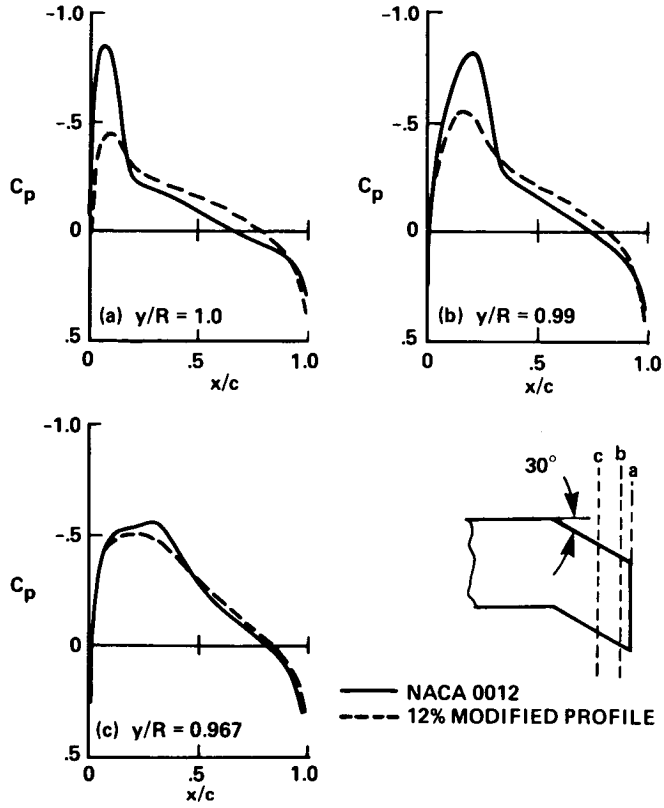

Figure 2.- Computed pressure distributions for a swept-tip planform. The NACA 0012 is seen to be unsuitable at the tip of this planform. Moving the maximum thickness point rearward at a point near the tip removes the strong shock there.

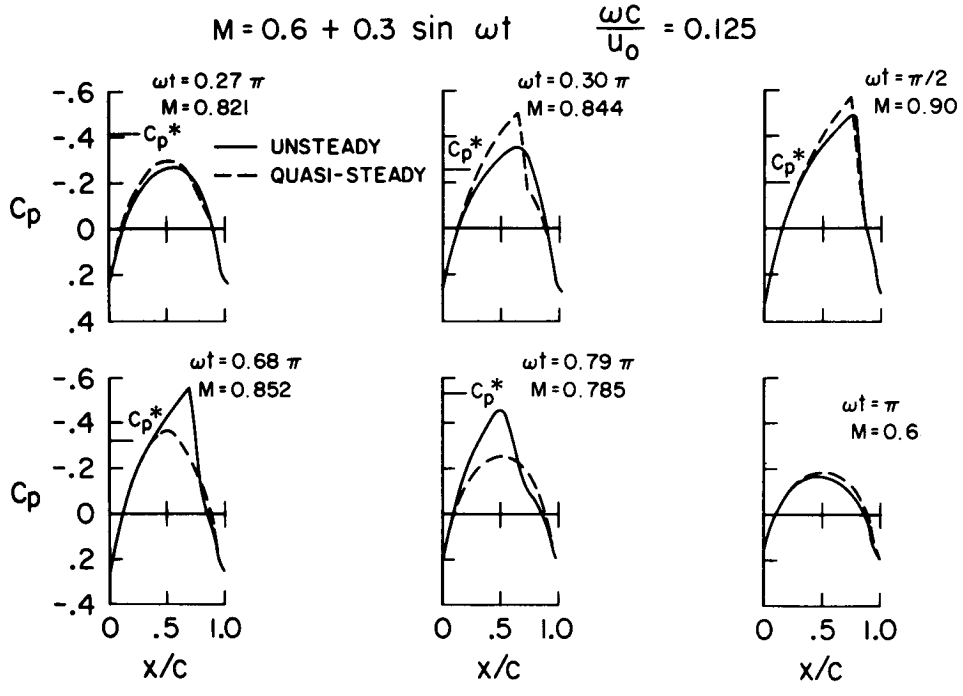

Figure 3.- The first computations of three-dimensional, unsteady rotor flows in the mid-70s showed a pronounced difference between steady and unsteady results.

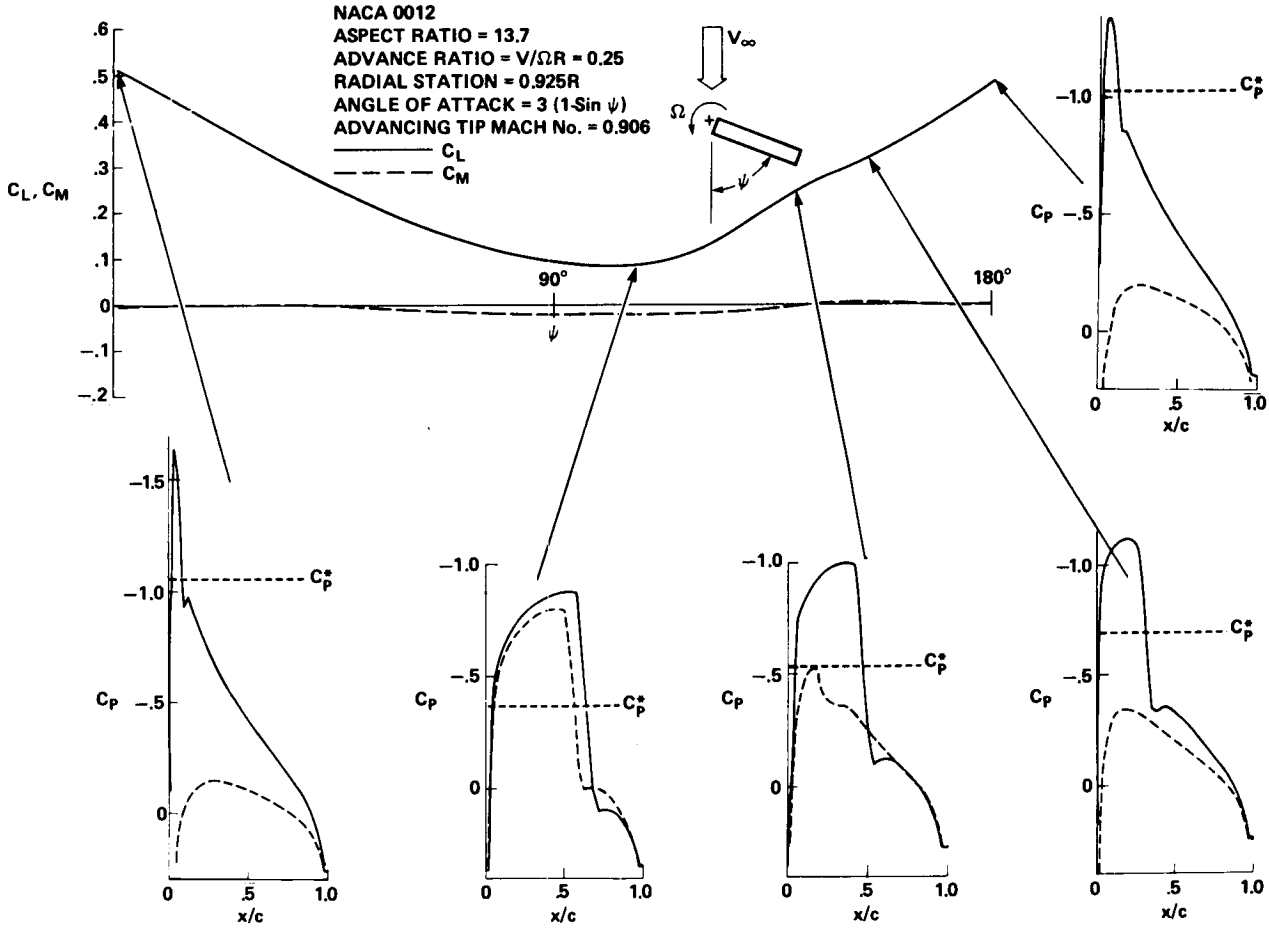

Figure 4.- A computed load variation on a helicopter rotor. By the later 1970s, hypothetical computations included both the effects of varying Mach number and lift. These computations further demonstrated the importance of unsteadiness.

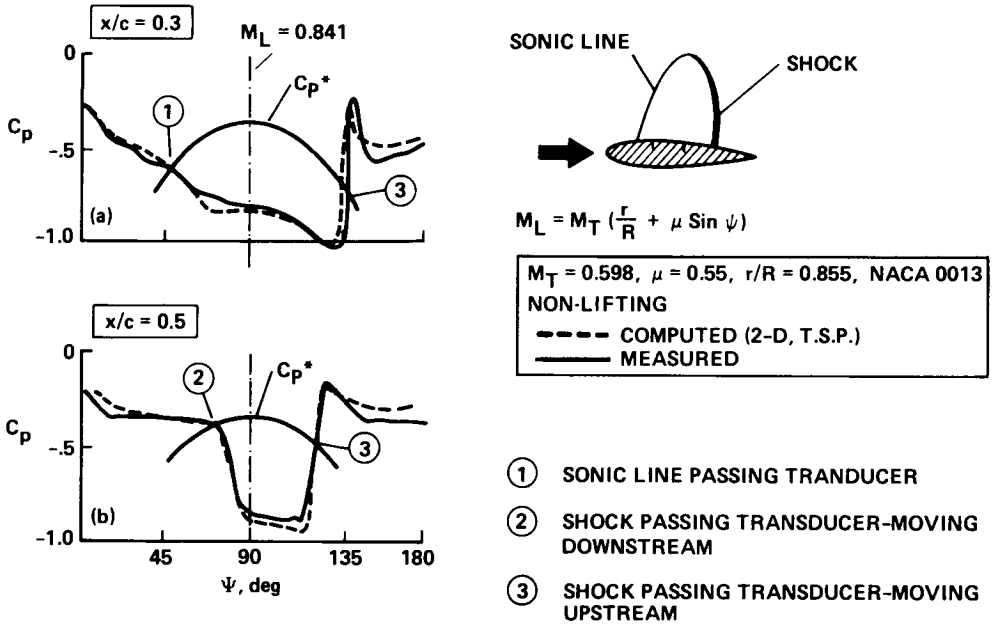

Figure 5.- The first experimental verification of computed transonic rotor flows. This nonlifting comparison further demonstrates transonic unsteadiness in the asymmetric shock motion about $\psi = 90°$.

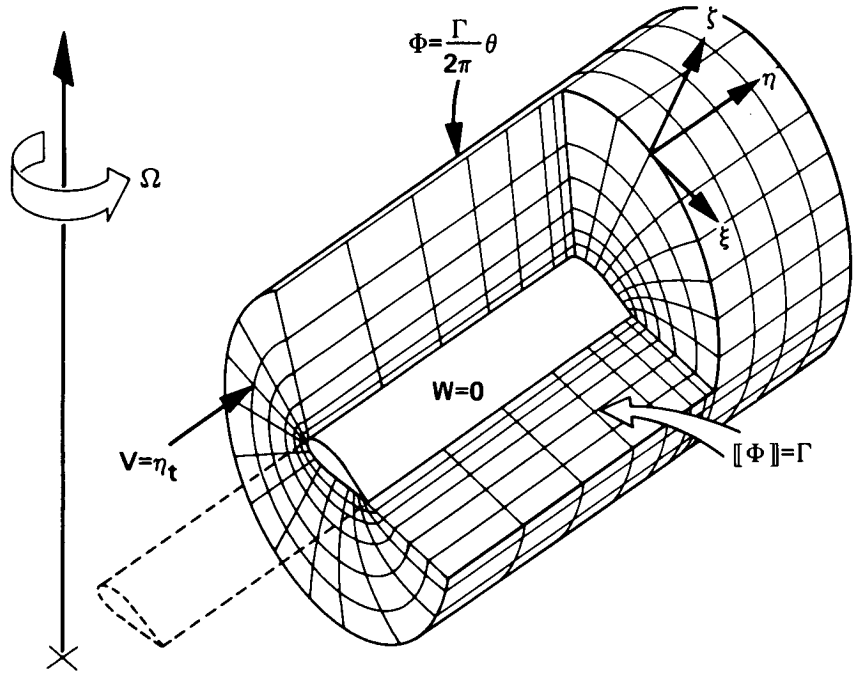

Figure 6.- Grid and boundary conditions for a local rotor computation. Up to the present all rotor CFD computations use a grid topology which is designed only to resolve flows near the blade surface.

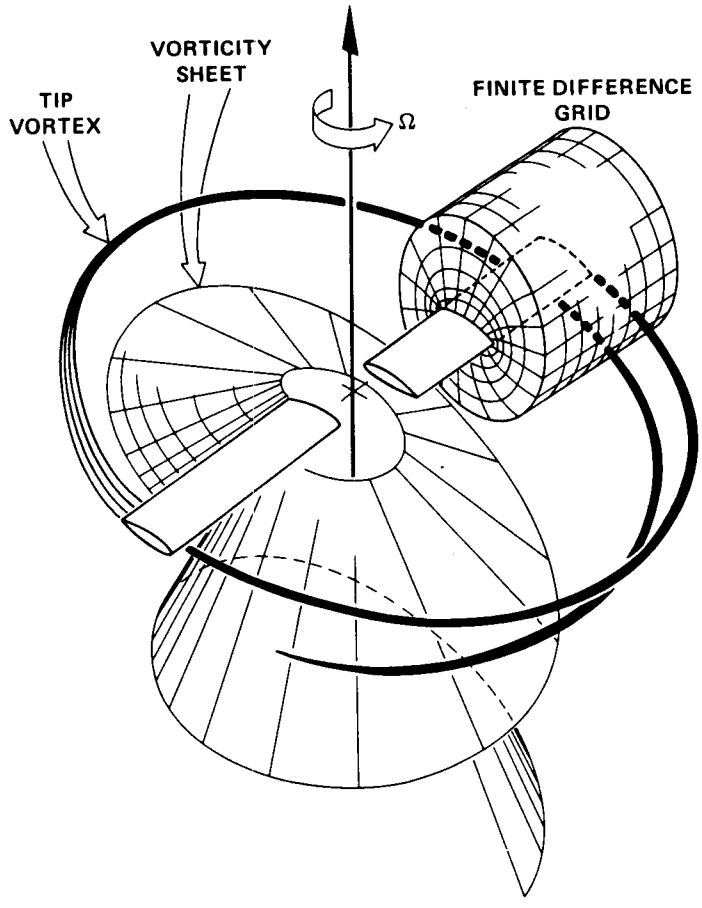

Figure 7.- A finite-difference grid embedded in a global flow region. The local blade grid can resolve only the most immediate wake features. These features must be accounted for by means other than grid resolution.

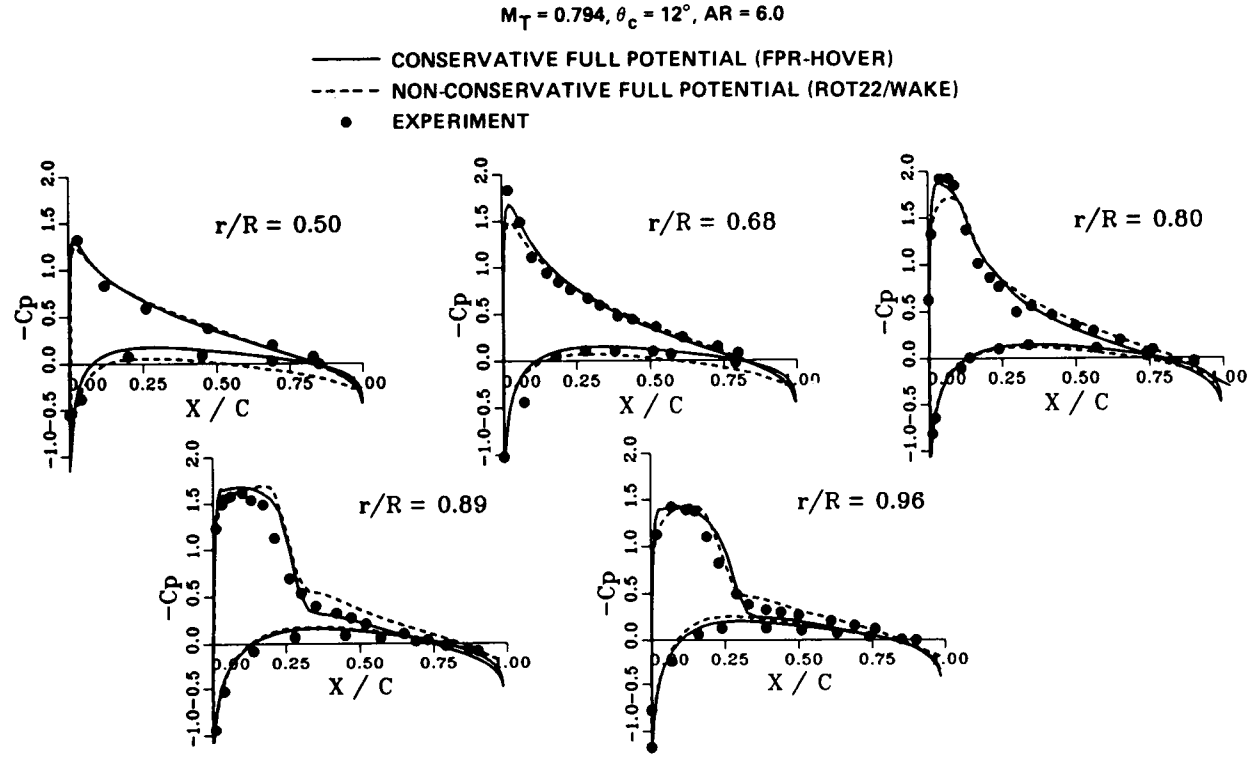

Figure 8.- Experimental verification of transonic computations for a hovering rotor. These computations employ various schemes to model the near and far wake details.

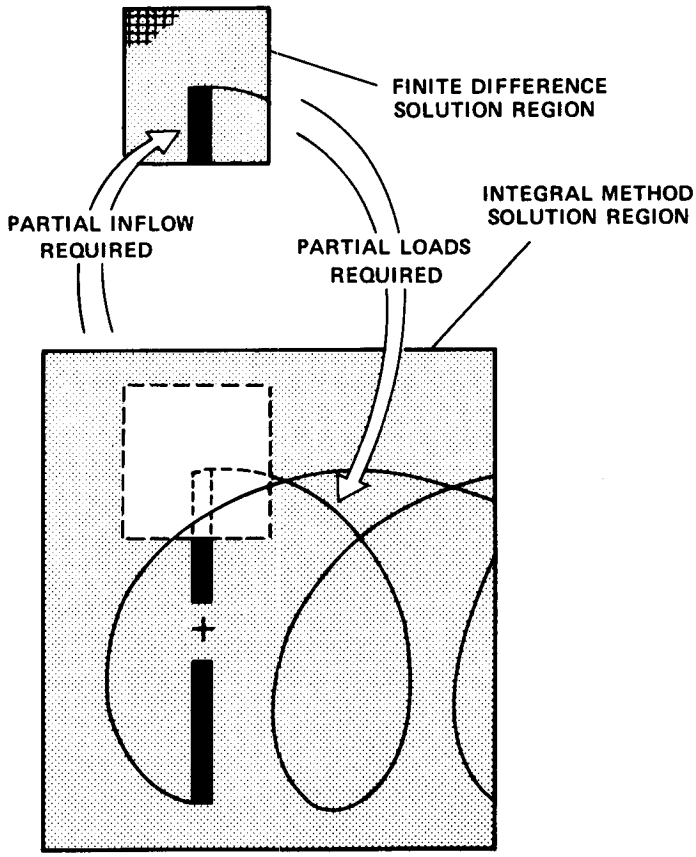

Figure 9.- Matching of local grids with advancing rotor wake system.

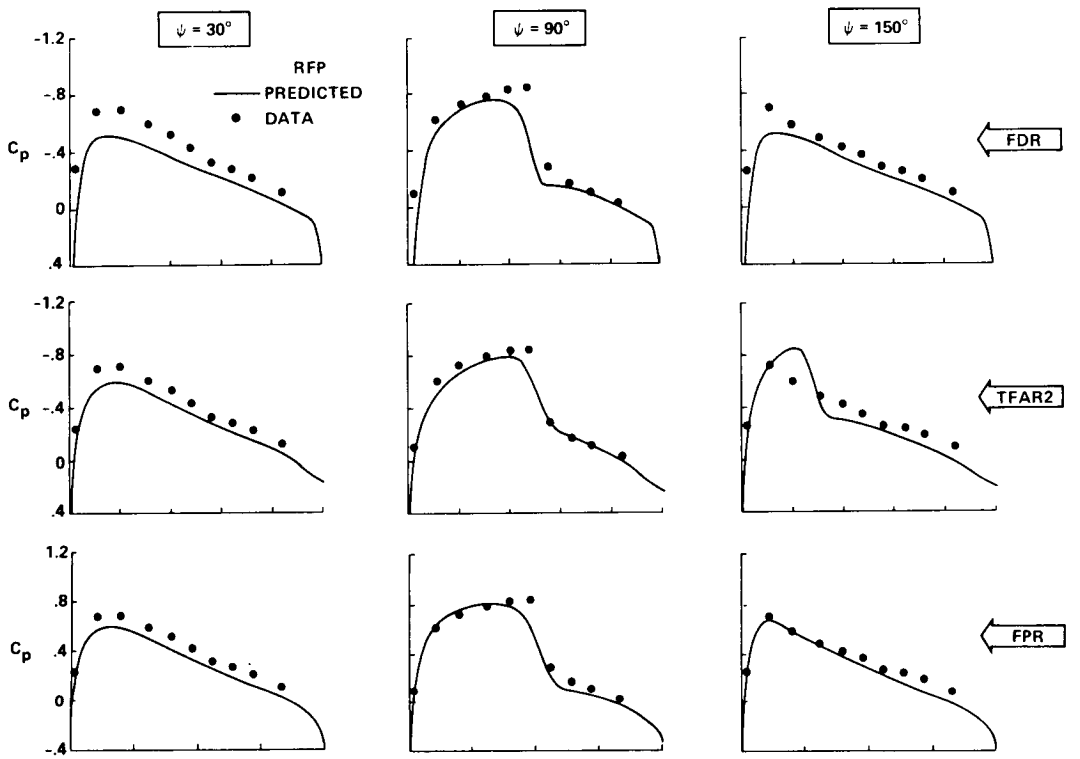

Figure 10.- A comparison of various computations with nonlifting rotor data.

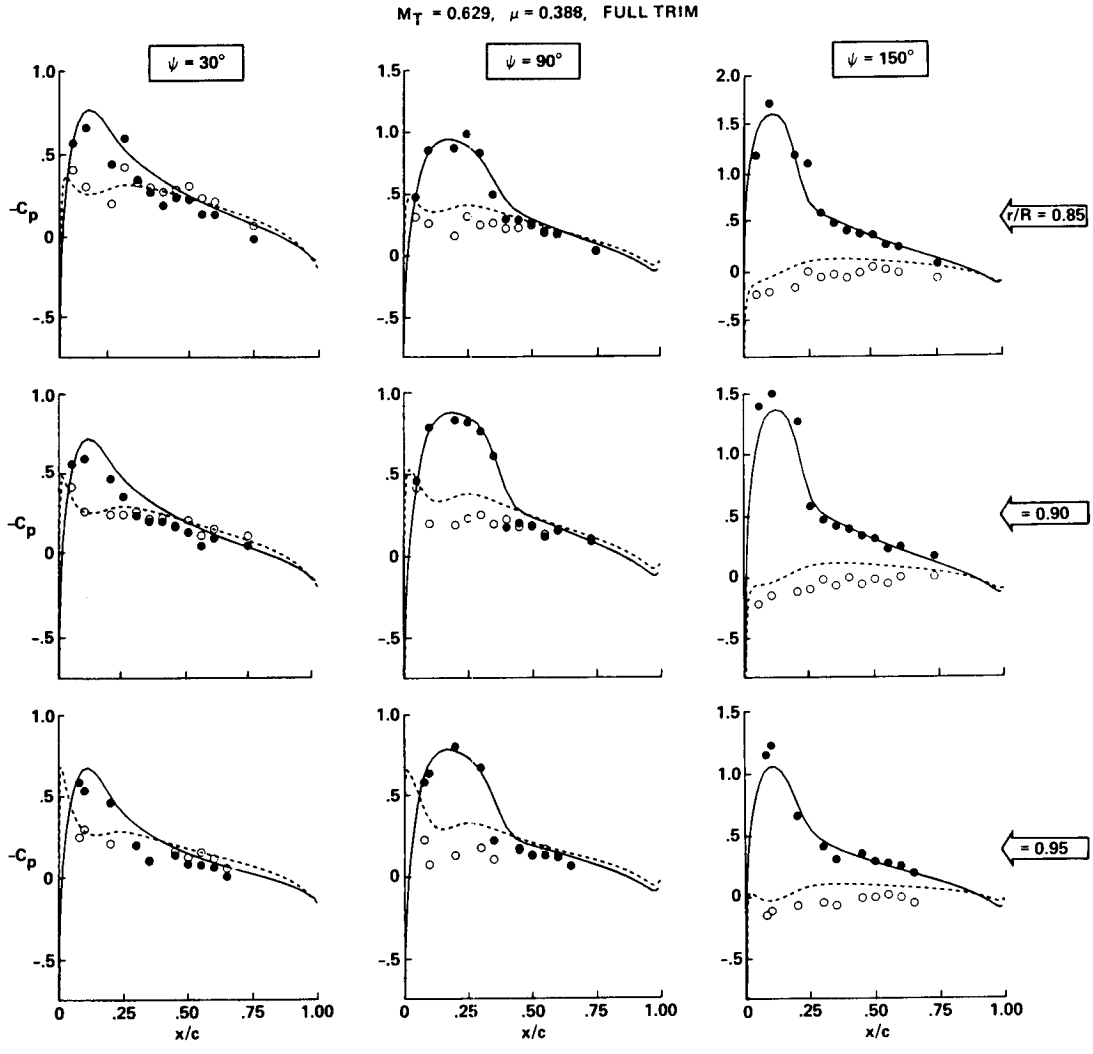

Figure 11.- A comparison of CAMRAD/FPR computations with lifting rotor data--ONERA 3-blade model.

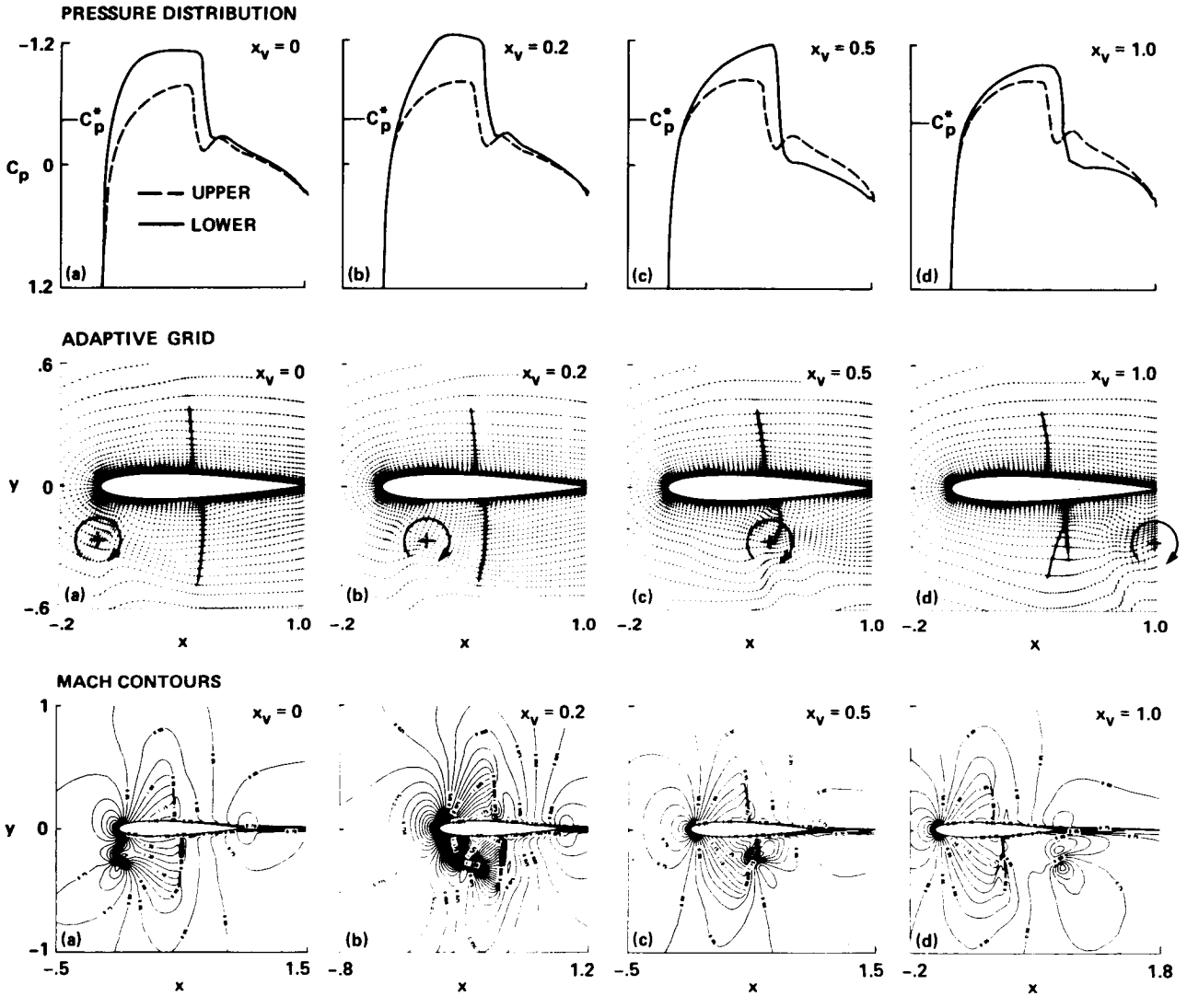

Figure 12.- Instantaneous surface pressure distributions, adaptive grid, and pressure contours for airfoil-vortex interaction; NACA 0012, $M_\infty = 0.80$, $\alpha = 0$, $\Gamma_v = 0.20$, $y_v = -0.26$.

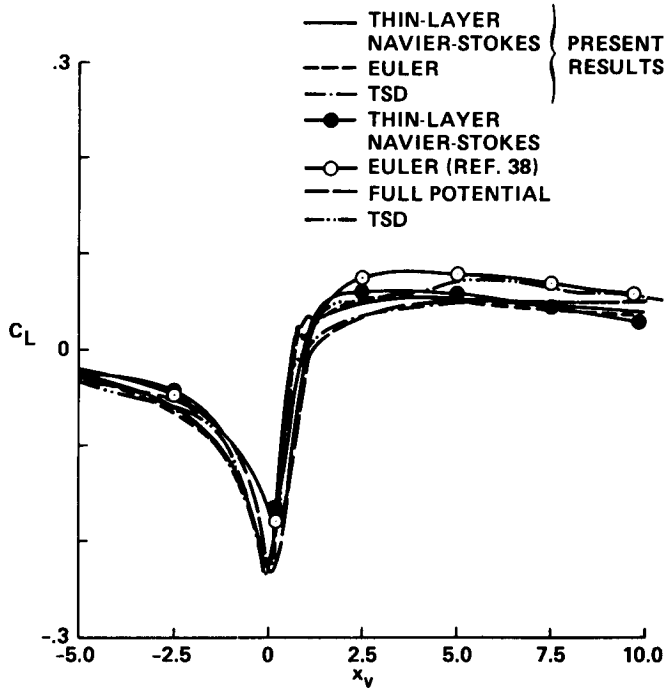

Figure 13.- Comparison of calculated lift coefficients from different methods for the case of figure 12.

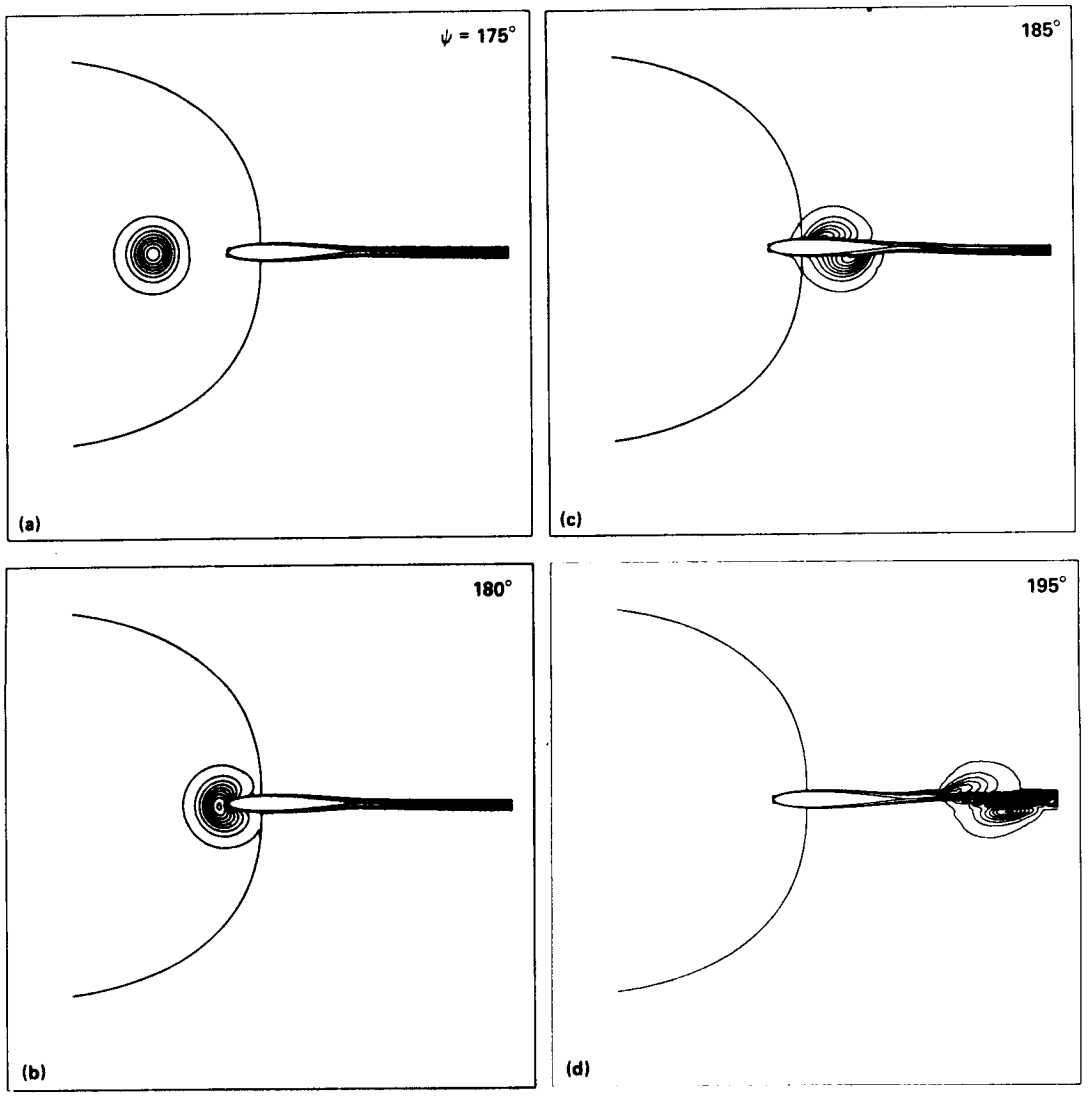

Figure 14.- Vorticity contours at various azimuthal angles for the case y_v = 0.0 in. and M_∞ = 0.536. (a) ψ = 175.00°; (b) ψ = 180.00°; (c) ψ = 185.00°; (d) ψ = 195.00°.

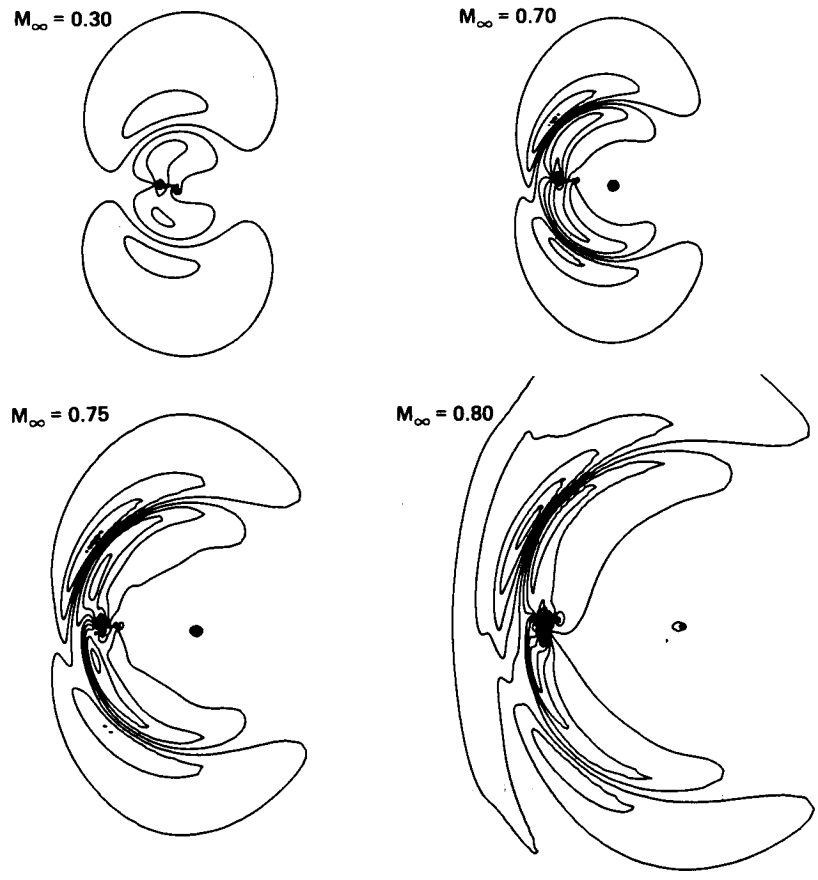

Figure 15.- Disturbance pressure contours, $(C_p - C_{pi})$ * Sqrt(R). NACA 0012 airfoil, y_v = -0.26, Γ_v = 0.20.

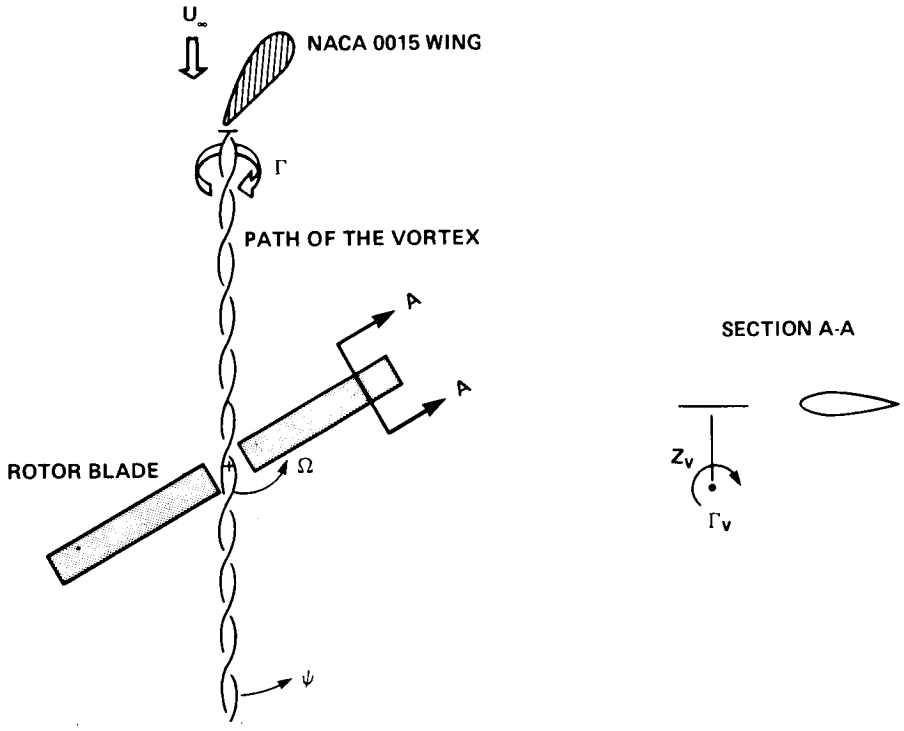

Figure 16.- Rotor-vortex interaction experiment described in reference 30.

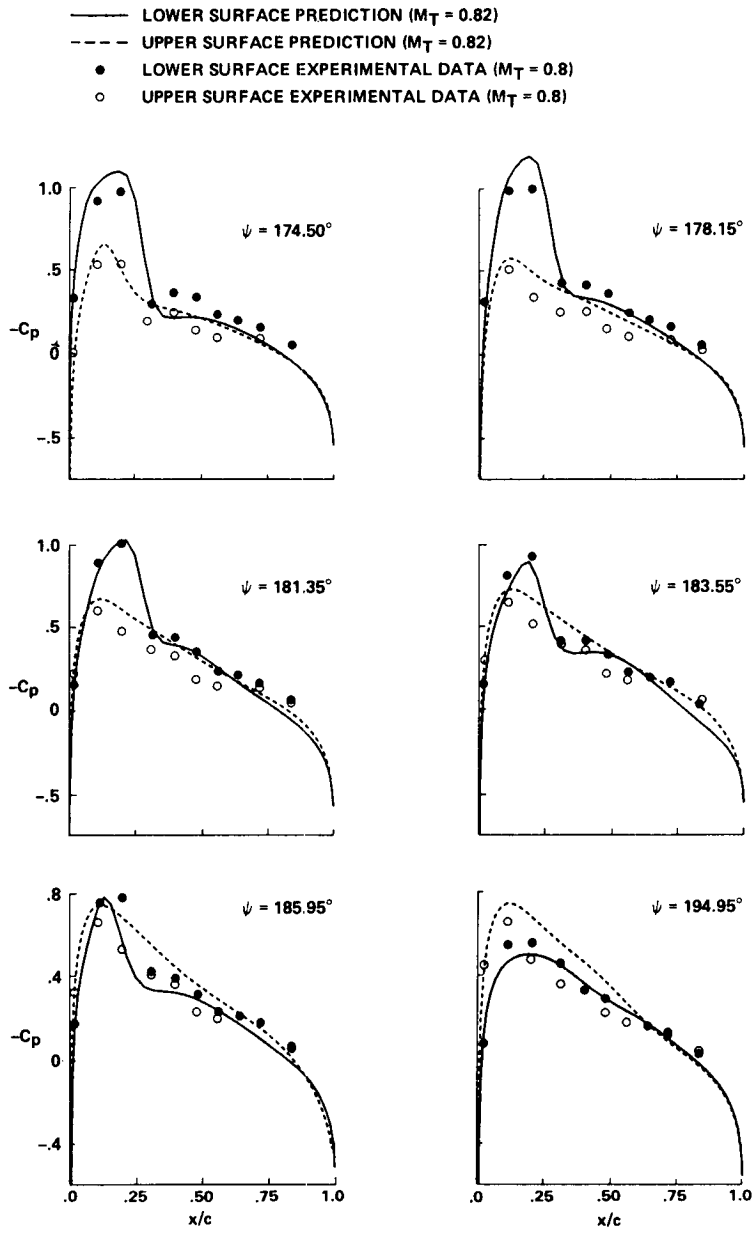

Figure 17.- Surface pressure results for a three-dimensional blade-vortex interaction, Γ_V = 0.177, Z_V/c = 0.4, μ = 0.2, AR = 7.0, r/R = 0.893, α = 0, untwisted, untapered, NACA 0012 blade. Data have M_T = 0.8, prediction is for M_T = 0.82.

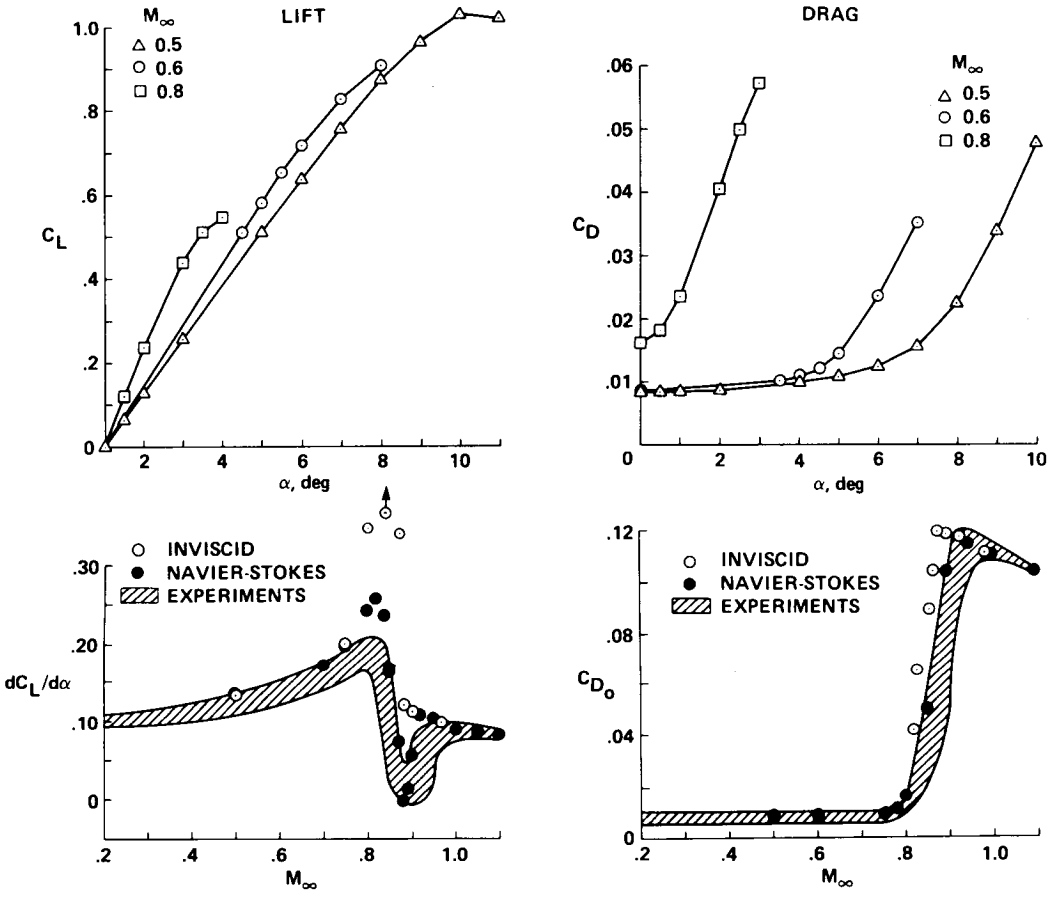

Figure 18.- Two-dimensional airfoil characteristics.

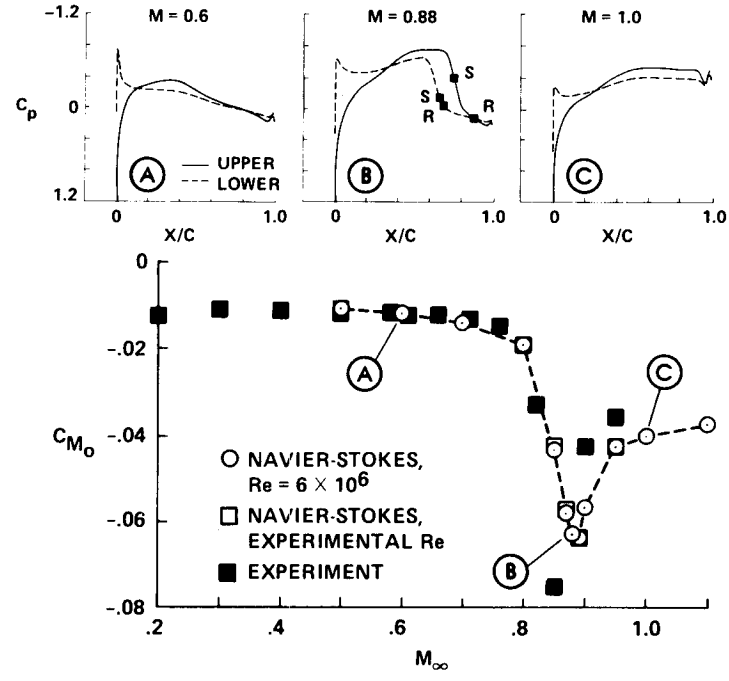

Figure 19.- Pitching moment vs. Mach number for the VR-8 airfoil at $C_L = 0$.

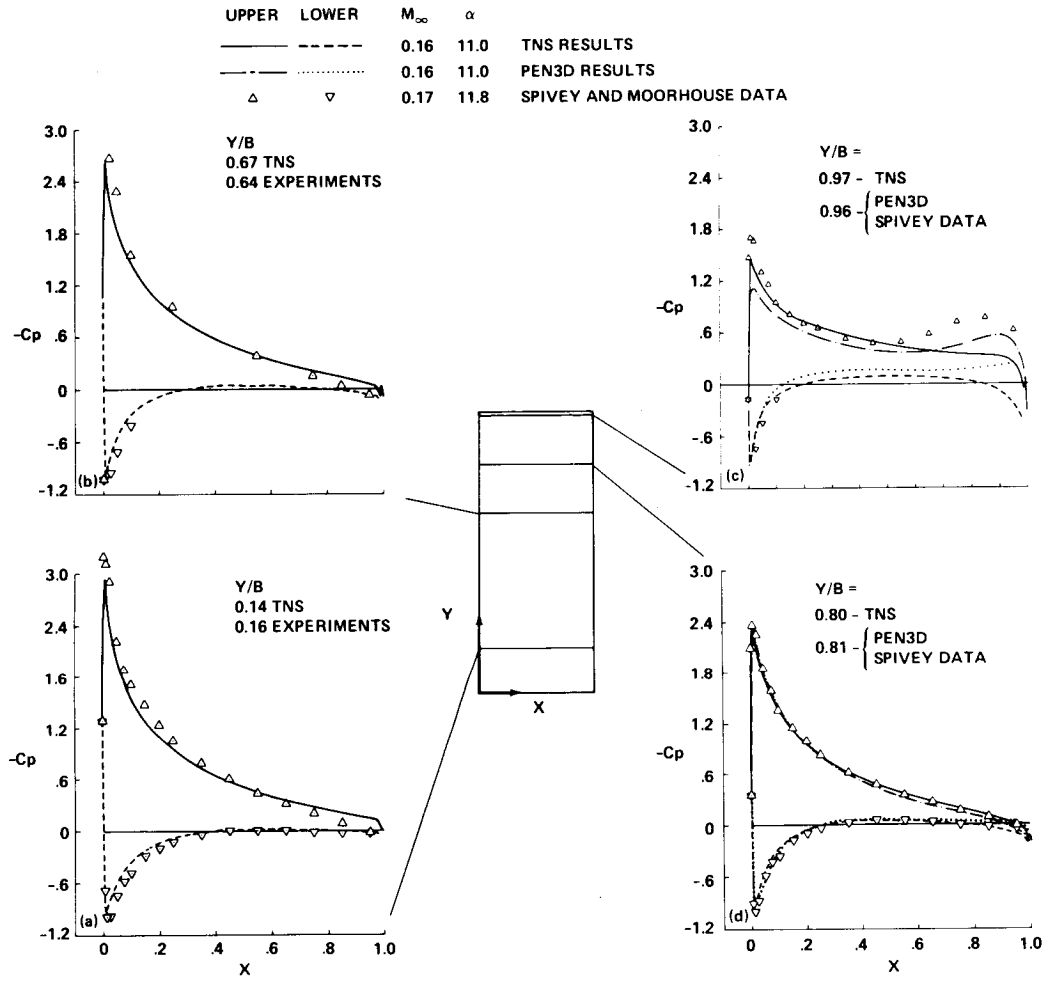

Figure 20.- Surface-pressure distributions for several spanwise stations and comparison with experimental data (refs. 16, 17) for NACA 0015 wing. M_∞ = 0.16, α = 11°, and Re = 2 million.

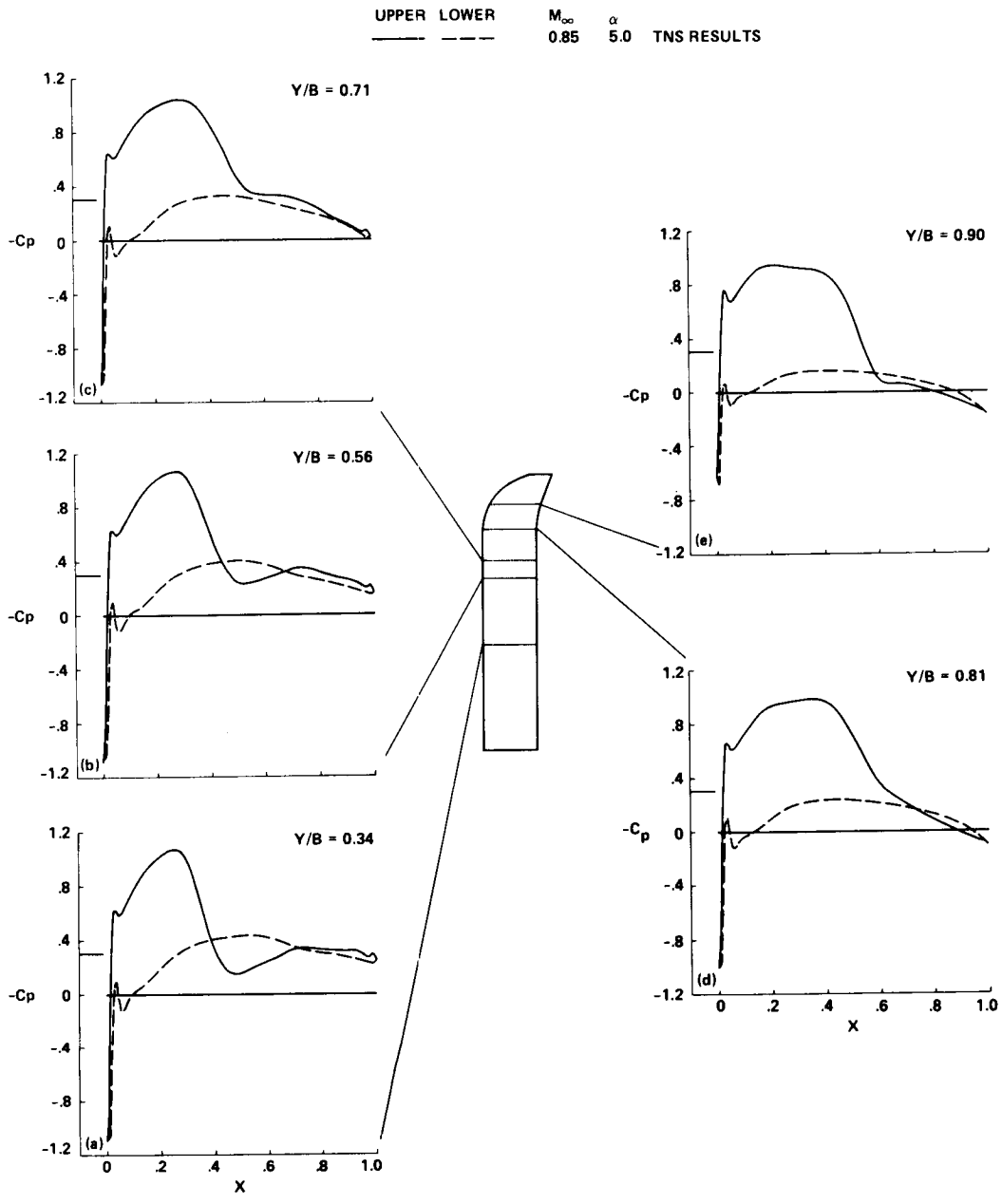

Figure 21.- Surface pressure distributions for the ONERA wing. M_∞ = 0.85, α = 5°, and Re = 8.5 million.

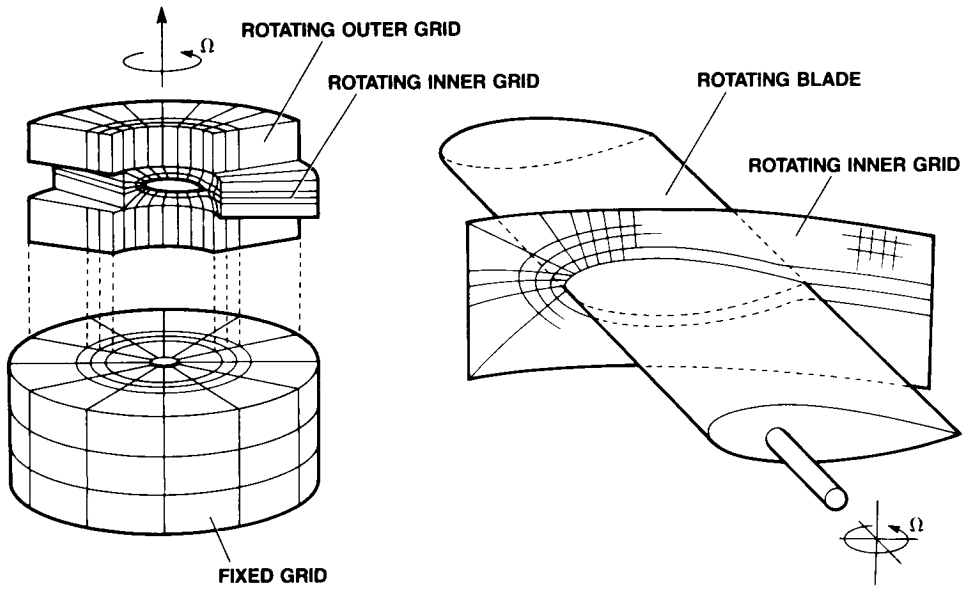

Figure 22.- Grid configuration for the computation of a complete helicopter.

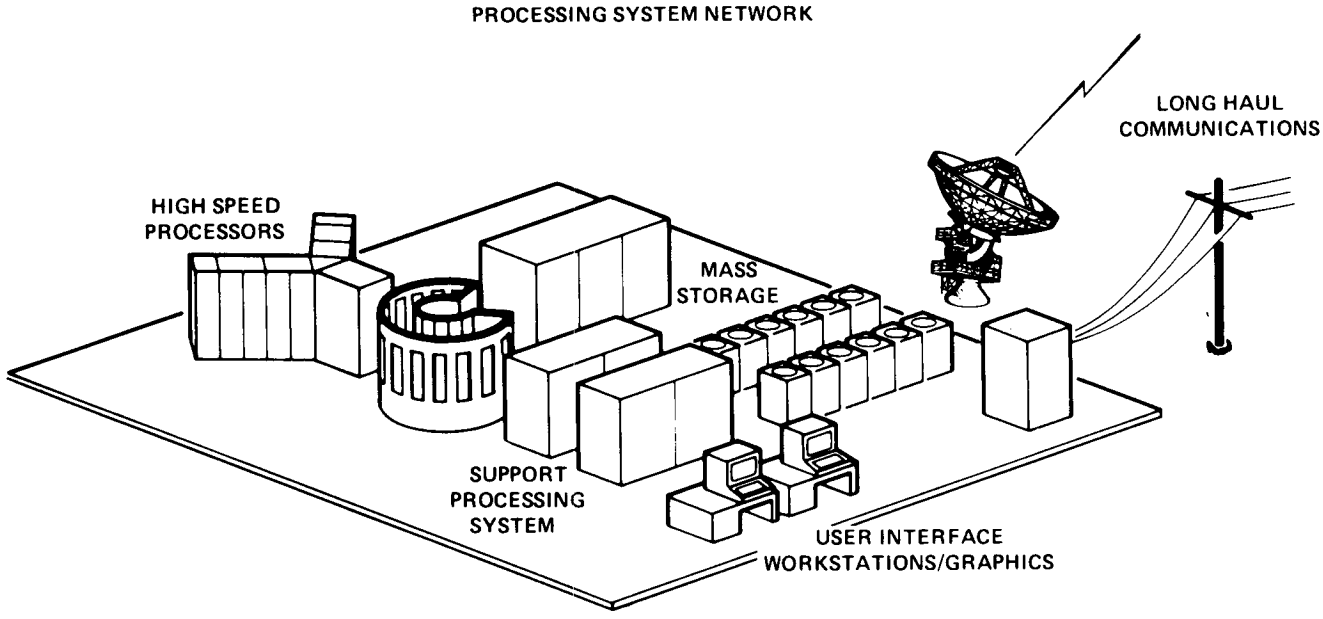

Figure 23.- NASA numerical aerodynamic simulation supercomputer project.